Magnetoresistance effects and phase coherent transport phenomena in a magnetic nonplanar two-dimensional hole system

Stefan Knott,* Thomas Ch. Hirschmann, Ursula Wurstbauer,† and Wolfgang Hansen
Institute of Applied Physics, University of Hamburg, D-20355 Hamburg, Germany

Werner Wegscheider
Solid State Physics Laboratory, ETH Zurich, CH-8093 Zurich, Switzerland

(Received 25 July 2011; revised manuscript received 3 October 2011; published 9 November 2011; publisher error corrected 23 November 2011)

Phase coherent transport phenomena are studied in a magnetic, two-dimensional hole system confined in a strained InAs quantum-well structure. At low magnetic fields we observe a well pronounced weak antilocalization signature, demonstrating that magnetic ions in proximity to the itinerant holes preserve phase coherent transport, although magnetic effects like the anomalous and planar Hall effects are present at low temperatures. From fits to the conductivity correction, spin and phase relaxation times are extracted in a large temperature range from 200 mK to 16 K. From the dependency of the spin relaxation time on temperature and in-plane magnetic fields, we conclude that the Dyakonov-Perel mechanism is the dominant spin relaxation mechanism. The metamorphic growth of the heterostructure causes a nonplanar quantum well that enables the formation of magnetic barriers in the presence of a parallel applied magnetic field. Transport through these magnetic barriers causes a positive magnetoresistance superimposed on the weak antilocalization signal.

DOI: 10.1103/PhysRevB.84.205302 PACS number(s): 73.20.Fz, 71.70.Ej, 75.47.−m, 75.50.Pp

I. INTRODUCTION

Spintronics offer novel opportunities for a new generation of devices combining standard microelectronics with the spin degree of freedom arising from the interaction between the spin and charge of the carriers.[1–3] Major challenges of spintronics include injection, manipulation, and detection of spin-polarized carriers. For both fundamental research and device applications, long spin relaxation times for carriers passing the crystal are essential. Promising candidates for electrodes realizing efficient spin injection and spin detection are diluted magnetic semiconductors[4,5] (DMSs) and ferromagnetic (half) metals.[1,6] To manipulate and control the spin of the itinerant charge carriers, attention is paid to two-dimensional charge carrier systems confined in semiconductors with strong spin-orbit interaction (SOI). SOI originates from bulk inversion asymmetry of the host material, the so-called Dresselhaus spin splitting[7] and from structure inversion asymmetry of the confinement potential, the so-called Rashba spin splitting.[8,9] SOI is more important in two-dimensional hole systems (2DHSs) compared to two-dimensional electron systems (2DESs) in most of the relevant materials because of the larger effective mass m^*.[10]

The SOI strength can be determined from, among other techniques, the beating pattern in the Shubnikov–de Haas (SdH) oscillations at larger magnetic fields[11–14] or at low fields from phase coherent transport phenomena such as weak antilocalization (WAL). At low magnetic fields WAL competes with the weak-localization (WL) effect.[15] The WL phenomenon emerges in magnetotransport measurements as a negative magnetoresistance that is caused by constructive interference of charge carriers scattered by the same group of defects on time-reversed closed paths. The phase change induced by a perpendicular magnetic field leads to a reduction of the constructive interference and accordingly to a negative magnetoresistance. In contrast, the coupling to the spin part of the wave function in the presence of SOI leads to a destructive interference of time-reversed closed paths at zero magnetic field. It was first investigated in three-dimensional systems and metal films[16] and was subsequently observed also in two-dimensional charge carrier systems in semiconductor heterostructures, like the 2DES in GaAs inversion layers[17] and in InGaAs/InAs quantum-well (QW) structures.[18] In recent years, 2DHSs in GaAs/AlGaAs QWs (Ref. 19) and in strained GaAs/InGaAs/GaAs QW structures[20] are also in focus due to their strong SOI strength. WL and WAL were also observed in diluted magnetic semiconductors, such as (Ga,Mn)As, demonstrating that phase coherent transport is not destroyed by magnetic impurities in direct proximity to the itinerant charge carriers.[21] GaMnAs and similar Mn-doped ferromagnetic semiconductors can be seen as dirty metals because of the required high doping concentration in the range of 10^{21} cm^{-3} and hence the short mean free path of the carriers. Consequently, these materials can serve as ferromagnetic electrodes for spin injection and detection[22] but are less well qualified for spin transport.

In this paper, we investigate the influence of a spatially separated, thin manganese-doped DMS layer on spin and phase relaxation times of a high-mobility 2DHS confined in a strained InAs QW. A unique property of our heterostructure is that the thin DMS layer, which is insulating at low temperatures, is used to provide the free holes for modulation doping of the InAs QW.[23] The narrow-band-gap semiconductor InAs as host material of the magnetic 2DHG features advantageous properties such as a large g factor and large Rashba-induced spin-orbit coupling.[14,24,25] The magnetic impurities in close proximity to the QW influence the magnetotransport properties at low magnetic fields and low temperatures, resulting in hysteretic behavior in longitudinal and transverse resistance.[26] Here we focus on the question of what happens to quantum interference effects if Mn ions are spatially separated but still in proximity to charge carriers of a high-mobility 2DHS.

At low temperatures ($T < 4.2$ K), we observe magnetic properties such as the anomalous Hall effect (AHE) and planar Hall effect (PHE), indicating interaction between Mn ions and free holes. In this temperature range, the WAL signature seems to have an anisotropic magnetoresistance (AMR) superimposed on it. Above $T \geqslant 4.2$ K, the AHE and PHE are suppressed and the phase coherent transport is uninfluenced. The characteristic spin relaxation time τ_{so} is comparable to the value in nonmagnetic 2DESs (Ref. 25) and nonmagnetic 2DHSs.[19,20]

II. SAMPLE DESIGN AND EXPERIMENTAL SETUP

We have investigated the low-field magnetoresistance on a Mn-modulation-doped InAs/$In_{0.75}Ga_{0.25}As$/$In_{0.75}Al_{0.25}As$ QW structure grown by molecular beam epitaxy (MBE). In Fig. 1(a) the layer sequence is sketched. A compositionally graded metamorphic buffer layer is deposited on semi-insulating (001) GaAs to form a virtual, lattice-matched substrate for the $In_{0.75}Ga_{0.25}As$ barrier. The active region consists of an InAs QW embedded in an $In_{0.75}Ga_{0.25}As$ QW structure. The thin (7 nm) Mn-doped $In_{0.75}Al_{0.25}As$ DMS layer providing the carriers for the 2DHS is inserted in the $In_{0.75}Al_{0.25}As$ barrier at 7.5 nm distance from the 4-nm-wide InAs QW hosting the 2DHS. The Mn doping concentration is about 10^{20} cm^{-3}; the doped layer is grown after the active region. Since the active layer is grown before the Mn doping [see Fig. 1(a)] we do not expect the presence of magnetic ions in the QW or spacer.[23] Further details on the heterostructure and growth can be found elsewhere.[23]

L-shaped Hall bar devices were defined using standard photolithography and wet chemical etching along the [110] and [$\bar{1}$10] crystallographic directions. The width of the paths are 200 μm and the distance between adjacent voltage probes is 1000 μm. In and Zn alloyed at about 350 °C is used for preparation of electrical contacts with Ohmic behavior.

Magnetotransport measurements were performed in four-probe geometry using standard low-frequency lock-in techniques. The excitation current was 100 nA at a frequency of 19.5 Hz. It was reduced to 50 nA for experiments at millikelvin temperatures to avoid sample heating. This was controlled by a careful analysis of the temperature-dependent development of the amplitude of the SdH oscillation.

Well pronounced integer quantum Hall effect and SdH oscillations prove the high quality of our samples, as shown

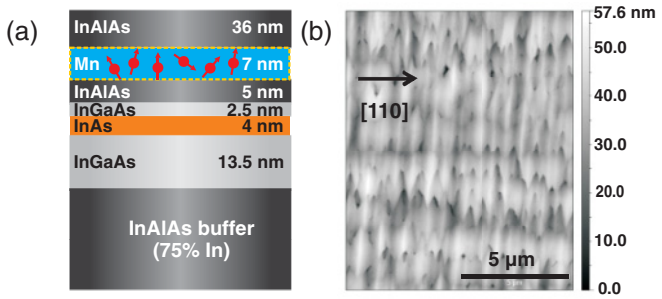

FIG. 1. (Color online) (a) Scheme of the layer sequence of the QW structure. (b) AFM image of the anisotropic cross-hatched surface morphology.

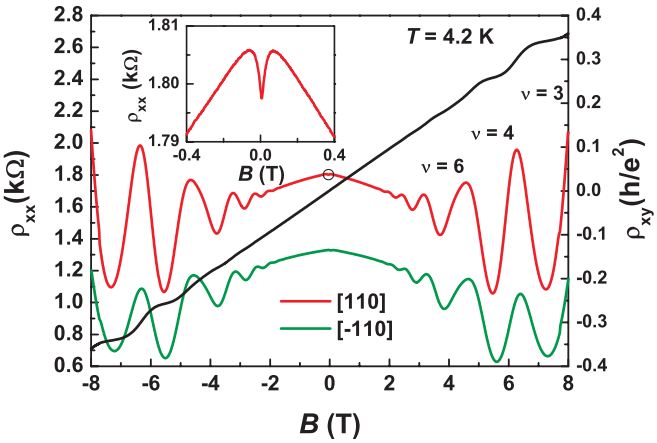

FIG. 2. (Color online) Hall resistance trace ρ_{xy} (black line, right vertical axis) and longitudinal magnetoresistance ρ_{xx} for currents along the anisotropic [110] (red line, left vertical axis) and [$\bar{1}$10] (green line, left vertical axis) directions at $T = 4.2$ K. The inset shows a magnification of the low-field region of ρ_{xx} displaying weak antilocalization.

in Fig. 2. The straight Hall slope over the whole magnetic field range and the periodicity in the SdH oscillations indicate the absence of parallel conductance in the thin DMS layer, or a second populated subband. In accordance with previous observations on electronic systems in $In_{0.75}Ga_{0.25}As$ metamorphic 2DESs,[27,28] the longitudinal resistance is anisotropic. The anisotropy in transport mobility μ can be associated with a lateral variation of the In concentration, which reveals different correlation lengths in the [110] and [$\bar{1}$10] crystallographic directions.[28] This anisotropic cross-hatched structure is displayed in an atomic force microscopy (AFM) image in Fig. 1(b).

At $T = 4.2$ K, the two-dimensional carrier density $p = 5.45 \times 10^{11}$ cm^{-2} and the mobility $\mu = 9.7 \times 10^3$ and 7.3×10^3 cm^2/V s for the [$\bar{1}$10] and [110] directions, respectively.

In the low-field region, a WAL signature is observed as shown in the inset of Fig. 2. The observation of a clear WAL signature indicates the presence of strong spin-orbit coupling, as expected for our heterostructure, and exhibits that $\tau_e < \tau_\phi$, where τ_ϕ is the phase coherence time. At about $B = 70$ mT a transition from positive to negative magnetoresistance reflects a crossover from WAL to WL.

III. MAGNETIC PROPERTIES

At temperatures below 4.2 K and at low magnetic fields, anomalous hysteretic contributions to the longitudinal and transversal resistivities are observable in the magnetoresistance traces, indicating spontaneous (ferro)magnetic ordering in the heterostructure. We attribute the observations to a contribution of the anomalous and planar Hall effects in the Hall resistance ρ_{xy} and a superposition of the WAL and an anisotropic magnetoresistance in the longitudinal resistance in ρ_{xx}.[26] These effects will be discussed in more detail in the following.

In Fig. 3, we display Hall resistance traces for different temperatures, revealing at high magnetic field the integer quantum Hall effect. At low magnetic fields and low temperatures, a local maximum in the magnetoresistance at zero

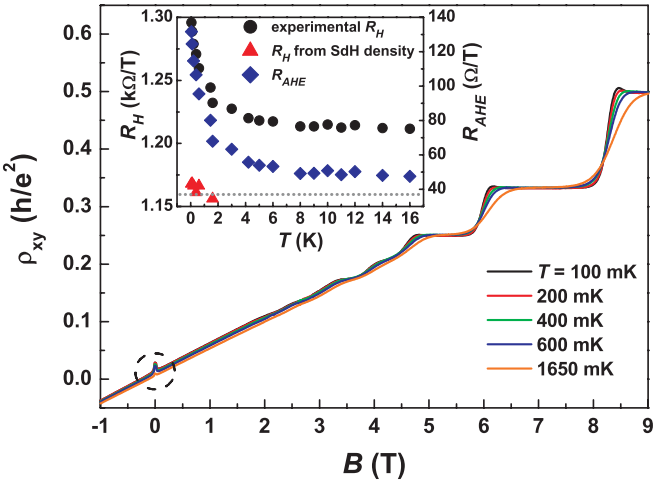

FIG. 3. (Color online) Hall resistance traces taken at temperatures between 100 mK and 1.65 K. Bending and fan out at lower magnetic fields indicate a superposition of ordinary and anomalous Hall effect. Upper left inset: Ordinary Hall coefficient R_H deduced from $1/B$ periodicity of the SdH oscillations (red triangles), R_H deduced from the measured Hall slope (black circles), and anomalous Hall coefficient R_{AHE} (blue diamonds) as a function of T.

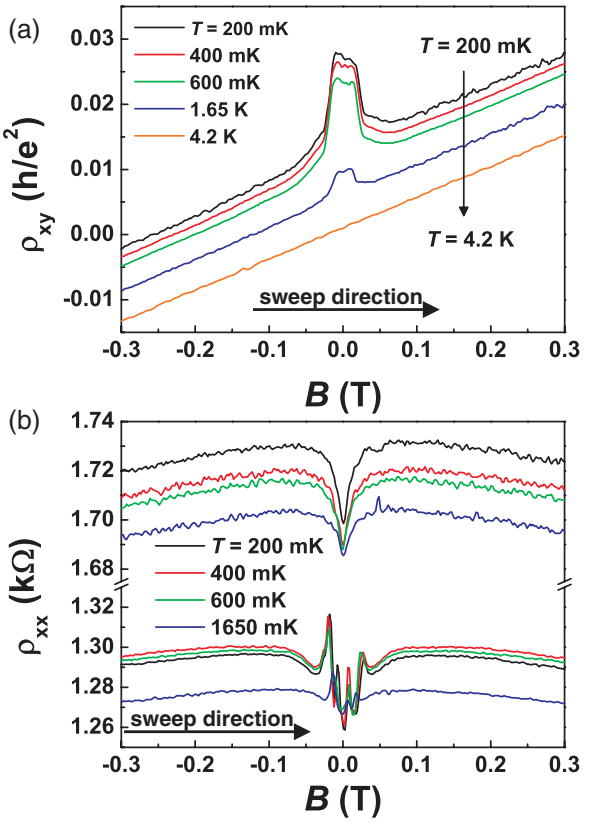

FIG. 4. (Color online) Low-field region of the Hall trace ρ_{xy} showing a superposition of ordinary, anomalous, and planar Hall effects. (a) Anomalous and planar Hall effects are reduced by increasing the temperature from 200 mK to 4.2 K. (b) Longitudinal resistance for currents along [110] (upper set of traces) and [$\bar{1}$10] (lower set of traces) directions for various T. Sweep direction of the magnetic field is from negative to positive for all measurements shown.

B and an offset in ρ_{xy} are observed [Fig. 4(a)]. Both signatures decrease with increasing T and vanish for $T \geqslant 4.2$ K. These effects are reminiscent of a PHE in epitaxial (Ga,Mn)As.[29] A careful analysis of ρ_{xy} shows hysteretic behavior with respect to the magnetic field sweep direction, as reported in a previous publication on a similar sample.[26] The presence of the PHE indicates a spontaneous magnetization in the (001) plane of the nonplanar heterostructure. We mention that the critical temperature T_c at which the PHE vanishes seems to be distinctly higher compared to the sample in Ref. 26 with $T_c = 600$ mK. In comparison to that heterostructure, our sample has a slightly higher Mn concentration and slightly lower mobility.

The PHE is mostly accompanied by an anisotropic magnetoresistance in the longitudinal resistance ρ_{xx}. In the sample investigated here, such AMR, superimposed on a weak antilocalization signature, is observed only in the [$\bar{1}$10] direction at low magnetic fields and for $T < 4.2$ K, whereas along the [110] direction the AMR seems to be almost fully suppressed. Again, similar behavior has been reported in Ref. 26, but with a superposition of AMR and WAL along both the [110] and [$\bar{1}$10] directions. The difference in the values of T_c and the suppression of AMR along the [110] direction of the sample investigated here might be caused by the difference in Mn doping concentration and mobility and hence changes in the strength of the WL or WAL effect.

At larger magnetic fields ($B < 0.2$ T), where the PHE no longer influences the transverse resistance, ρ_{xy} is linear in B, with a slope reflecting the ordinary Hall coefficient $R_H = (pe)^{-1}$. Although there is no significant variation in the low-dimensional carrier density p determined from SdH measurements ($p = 5.35 \times 10^{11}$ cm^{-2}) for $0.1 < T < 1.6$ K, R_H clearly decreases between 0.1 and 6 K and gradually saturates for higher temperatures as depicted in the inset of Fig. 3. The Hall coefficient converges to a value of $R_H \approx 1.21$ kΩ/T, a higher value than expected from the density of the SdH oscillations. The temperature dependency of R_H can be attributed to the relation of the anomalous Hall effect to ρ_{xy}, which follows the empirical expression[30]

$$\rho_{xy} = R_H B + R_{\mathrm{AHE}} M. \tag{1}$$

Here the first term is the contribution of the ordinary Hall effect, usually nearly temperature independent and proportional to the magnetic field B. The second term is the anomalous Hall effect and is proportional to the magnetization M of the system.

The anomalous Hall coefficient R_{AHE} can be described by means of the longitudinal resistance ρ_{xx}:[30]

$$R_{\mathrm{AHE}} = a\rho_{xx} + b\rho_{xx}^2, \tag{2}$$

where the linear term originates from skew scattering and the quadratic term from side-jump scattering and/or additional intrinsic effects.[31] In order to evaluate our data, a temperature-dependent offset in ρ_{xy} [see Fig. 4(a)] must be compensated, whose origin is ascribed to the superimposed planar Hall effect. With respect to this temperature-dependent constant summand, the anomalous Hall constant R_{AHE} can be extracted from the data using Eq. (1) and the linear and quadratic contributions of ρ_{xx} to R_{AHE} with the help of Eq. (2). The

temperature-independent values of a and b are 0.2 T^{-1} and -8×10^{-5} $(T\ \Omega)^{-1}$, respectively. Fits without the quadratic term differ only marginally from fits with both parameters. Within the uncertainty of experiment and fit, the quadratic contribution to R_{AHE} seems to be negligible, and consequently the anomalous Hall effect is dominated by the skew scattering in our heterostructure, in accordance with calculations for a magnetic 2DES with Rashba SOI and pointlike defects in the weak-scattering limit.[31]

We observe that the Mn concentration, 2D hole density, mean free path, and also small variations in the distance between the 2D system and the magnetic doping layer due to standard thickness variations in MBE growth strongly influence the Curie temperature in the doping layer and the magnetoresistance in our 2DHGs. Whereas the influence of the long-range-ordered doping layer on the Hall resistance, mainly the superimposed planar Hall effect, is very robust and much less influenced by the parameters listed above, ρ_{xx} seems to be very sensitive to small changes in these parameters. Our results indicate that those small changes can cause hysteretic AMR effects to compete with WAL signatures.

For both samples, the measured Hall resistivity at $T < T_c$, here $T < 4.2$ K, is a superposition of ordinary, anomalous, and planar Hall effects, whereas for $T > T_c$ (here $T > 4.2$ K) the ordinary Hall effect dominates. This demonstrates that the additional anomalous contributions to the longitudinal and transverse resistance are due to magnetic ordering, most likely in the Mn doping layer. The critical temperature T_c can be influenced by the Mn doping concentration, as intuitively expected.

Furthermore, the weak AMR along [110] enables us to investigate WL effects in this sample and determine the spin relaxation time τ_{so} and phase relaxation time τ_ϕ at temperatures down to 200 mK.

IV. PHASE COHERENCE AND SPIN RELAXATION TIMES FROM WEAK ANTILOCALIZATION

A WAL signal is observable in the diffusive transport regime, where the mean free path of the carrier is much smaller than the phase coherence length. The quantum correction of the conductivity caused by WL and WAL phenomena is theoretically described by the models introduced by Hikami, Larkin, and Nagaoka[15] (HLN) and by Iordanski, Lyanda-Geller, and Perel[32] (ILP). A prerequisite for the HLN model is that the spin-splitting energy is cubic in k, whereas the ILP model incorporates spin-splitting terms both linear and cubic in k. If the k-linear terms are neglected, the ILP and HLN models exhibit the same results. From fitting the experimental data to the models, the spin relaxation time τ_{so} and phase relaxation time τ_ϕ can be extracted.

In the investigated heterostructure only states in the highest valence band are occupied, which for both InAs and GaAs QWs are heavy-hole states.[10] In contrast to conduction band states or light-hole states in the valence band, the spin splitting is determined by k^3 terms, k-linear terms have not to be taken into account.[10] Therefore it is appropriate using the HLN theory to fit the quantum correction to the magnetoconductivity resulting from the WAL phenomenon in our magnetic 2DHS.[19,20] Prior to the fitting procedure, a

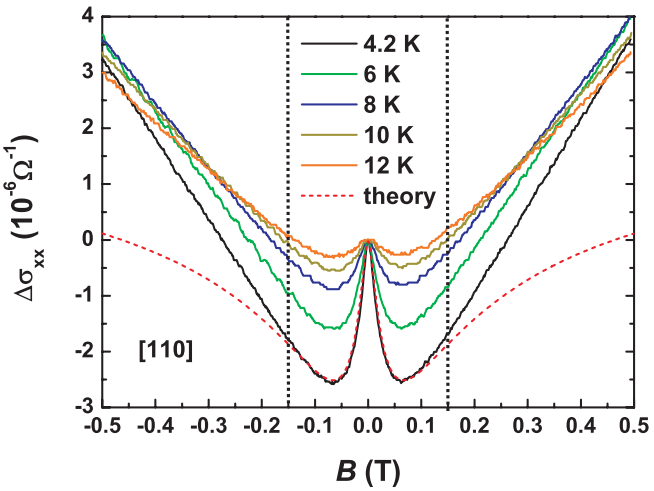

FIG. 5. (Color online) (a) Magnetoconductivity correction $\Delta\sigma_{xx} = \sigma_{xx}(B) - \sigma_{xx}(0)$ due to WAL for different temperatures in the low-field region along the [110] direction. For $T = 4.2$ K, the measured magnetoconductivity (black) and best fit to the data (dashed, red line) using the HLN theory are compared. A good agreement of the WAL model with the experimental data is expected for $|B| < 150$ mT, as indicated by the vertical dashed lines.

background consisting of a parabolic negative magnetoresistance was subtracted from the measured data, as can be seen in Fig. 2. This parabolic background can be attributed either to carrier-carrier interaction[33] or to the presence of a system with two types of charge carrier with different mobilities.[19] The WAL and/or WL correction to the magnetoconductivity, $\Delta\sigma_{xx} = \sigma_{xx}(B) - \sigma_{xx}(0)$, is plotted for temperatures between 4.2 and 12 K on the example of the [110] direction in Fig. 5. The WAL signal decreases with increasing temperature and finally vanishes for temperatures above $T > 16$ K.

We use the following expression based on the HLN theory to fit our experimental data and to extract characteristic relaxation times:[15]

$$\Delta\sigma(B) = \frac{-e^2}{2\pi^2\hbar}\left[\Psi\left(\frac{1}{2}+\frac{H_e}{B}\right) - \Psi\left(\frac{1}{2}+\frac{H_\phi + H_{so}}{B}\right) - \frac{1}{2}\Psi\left(\frac{1}{2}+\frac{H_\phi}{B}\right) - \frac{1}{2}\Psi\left(\frac{1}{2}+\frac{H_\phi + 2H_{so}}{B}\right)\right]. \quad (3)$$

The characteristic fields are defined as follows:

$$H_e = \frac{\hbar}{4De\tau_e}, \quad H_\phi = \frac{\hbar}{4De\tau_\phi}, \quad H_{so} = \frac{\hbar}{4De\tau_{so}}. \quad (4)$$

The fields correspond to the scattering times of the elastic (τ_e), inelastic (τ_ϕ), and spin-orbit (τ_{so}) dephasing processes, respectively. B denotes the external perpendicular magnetic field, D the diffusion constant, and Ψ the digamma function. As demonstrated exemplarily by the red dashed line in Fig. 5 for data taken at $T = 4.2$ K on a Hall bar oriented along the [110] direction, the HLN fits to the magnetoconductivity correction $\Delta\sigma_{xx}$ are in excellent agreement with the experimental traces for $|B| < 150$ mT.

The conductivity minimum occurs according to Eq. (3) at a field of $\approx 2H_{so}$ if $H_{so} \gg H_\phi$.[17] The spin relaxation time τ_{so} is nearly temperature independent, because the minima in the

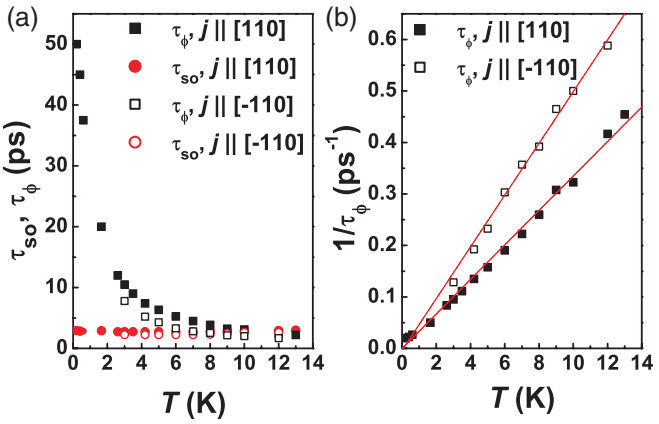

FIG. 6. (Color online) (a) Temperature dependence of the characteristic relaxation times for the [110] (filled symbols) and the [-110] direction (open symbols): spin relaxation τ_{so} (red circles) and phase relaxation τ_ϕ times (black squares). (b) τ_ϕ is distinguished by a linear $1/T$-dependence at higher T and a deviation toward lower values for $T = 1.4$K.

experimental traces in Fig. 5 hardly shift with temperature. The magnitude of the antilocalization peak is determined by the ratio of $H_{so}/H_\phi = \tau_\phi/\tau_{so}$. It is clearly visible in Fig. 5 that the phase relaxation time τ_ϕ strongly depends on temperature.

For a more quantitative comparison of the relaxation times the spin relaxation time τ_{so} and phase coherence times τ_ϕ from the HLN fits to the data are plotted as a function of temperature for both crystallographic directions in Fig. 6(a). Due to the pronounced superimposed AMR along [$\bar{1}$10], τ_ϕ and τ_{so} are evaluated only for $T > 3$ K. Along the [$\bar{1}$10] direction, τ_{so} is about 20% and τ_ϕ about 10% lower compared to the [110] direction, which is consistent with the lower mobility along the [110] direction. The values of τ_{so} are 2.75 and 2.15 ps for the [110] and [$\bar{1}$10] directions and are nearly temperature independent. These results strongly points toward the Dyakonov-Perel (DP) mechanism as the dominant spin relaxation mechanism, as is assumed in a degenerate charge carrier system in semiconductors with inversion asymmetry as is the case for InAs and InGaAs.[34] The characteristic fields corresponding to the SOI can be determined with the help of Eq. (4) and are determined as $H_{so} = 21.3$ mT for the [110] and $H_{so} = 15.7$ mT for the [$\bar{1}$10] crystal directions.

In Fig. 6(a), the phase relaxation time τ_ϕ increases with decreasing temperature from $\tau_\phi = 7.4$ ps at 4.2 K to $\tau_\phi = 50$ ps at 200 mK for the [110] direction. For temperatures above 600 mK, $1/\tau_\phi$ is a linear function of T [see Fig. 6(b)]. The linear temperature dependence of $1/\tau_\phi$ can be explained by phase relaxation caused by inelastic electron-electron (here hole-hole) interaction in the investigated temperature range.[35] Theoretically, τ_ϕ is expected to diverge as $T \to 0$ K. A possible origin for the deviation from the linear slope in the low-temperature range ($T < 600$ mK) could be the superimposed AMR in ρ_{xx}, the intrinsic fields due to the spontaneous magnetization in the doping layer,[36] or the interaction of the two-dimensional holes with the long-ranged-ordered DMS layer in close proximity.[37,38] We mention that the temperature of the 2D holes closely follows the bath temperature in the reported range as it is carefully controlled by the amplitude of the SdH oscillations.

At low temperature the dephasing rate τ_ϕ^{-1} of electrons in a 2DES can be described for $\sigma \gg e^2/\hbar$ by[39–41]

$$\tau_\phi^{-1} \approx \frac{e^2/\hbar}{\sigma} \ln\left(\frac{\sigma}{e^2/\hbar}\right) \frac{k_B T}{\hbar} = cT, \tag{5}$$

with the conductivity $\sigma = ep\mu$. The prefactor c can be ascertained by the slopes of the traces in Fig. 6(b). The calculated value [$c = 0.048$ (K s)$^{-1}$] is in excellent agreement with the slope determined from the experimental dephasing rate τ_ϕ^{-1} [$c = 0.050$ (K s)$^{-1}$] for $j \parallel$ [$\bar{1}$10]. In the direction with the higher mobility ($j \parallel$ [110]), a deviation between the calculated parameter [$c = 0.047$ (K s)$^{-1}$] and the value from the dephasing rate [$c = 0.034$ (K s)$^{-1}$] emerges, whose origin is unclear yet.

In comparison to a 2DEG in an identical heterostructure, where H_{so} has been reported to constitute 0.15 mT,[25] the SOI field is more than 100 times larger in the magnetic 2DHS reported here. On the other hand, the value of τ_{so} is comparable to those reported for electron systems in Si-doped $In_{0.75}Ga_{0.25}As/InAs/In_{0.75}Ga_{0.25}As$ QWs ($\tau_{so} \approx 3$ ps),[25] for hole systems in C-doped GaAs/AlGaAs QWs ($\tau_{so} \approx 3$ ps, but τ_ϕ differ by more than an order of magnitude),[19] and strained GaAs/InGaAs/GaAs QWs ($\tau_{so} \approx 11$ ps).[42] A precise quantitative comparison of the determined relaxation times with literature values is difficult due to differences in host materials, symmetry of confinement potentials, and carrier types and density.

V. INFLUENCE OF THE NONPLANARITY OF THE 2DHS: MAGNETIC BARRIERS

As mentioned in the previous section, the T dependency of τ_{so} provides an indication of the relevant spin relaxation mechanism, and we suggest that the Dyakonov-Perel scattering dominates as expected theoretically. Studying τ_{so} as a function of the in-plane magnetic field component $B_\parallel$ is another possibility to distinguish between the DP and Elliot-Yaffet (EY) scattering mechanisms.[43,44] In order to strengthen our interpretation that the DP mechanism is dominating, we have studied the magnetoresistance in tilted magnetic fields.

Magnetoresistance traces taken at $T = 4.2$ K are shown in Fig. 7 for a large range of tilt angles $0^\circ \leqslant \alpha \leqslant 88^\circ$ between the sample normal and the magnetic field, which is tilted in the [110] crystallographic direction. The magnetoresistance is plotted versus the perpendicular component of the magnetic field, $B_\perp$, to evaluate the impact of a parallel field on the WAL signal. In both crystallographic directions, WL and WAL signals are robust against tilt angles $\alpha \approx 80^\circ$ with respect to the sample normal. This proves that both quantum interference phenomena result from orbital motion of the charge carriers. The maximum in the resistance denoting the change from WAL to WL appears at $B_\perp \approx 70$ mT and constitutes roughly the value for $2H_{so}$.

For tilt angles α larger than 80° the magnetoresistances for currents along the [110] and [$\bar{1}$10] directions (upper and lower set of curves in Fig. 7, respectively) are significantly different. In particular, along the [$\bar{1}$10] direction, further increasing

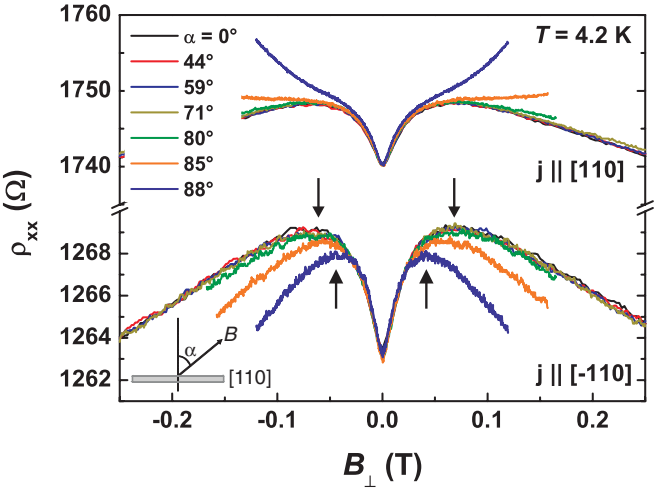

FIG. 7. (Color online) Tilted field measurements along the [110] (upper set of traces) and the [$\bar{1}$10] directions (lower set of traces) at $T = 4.2$ K.

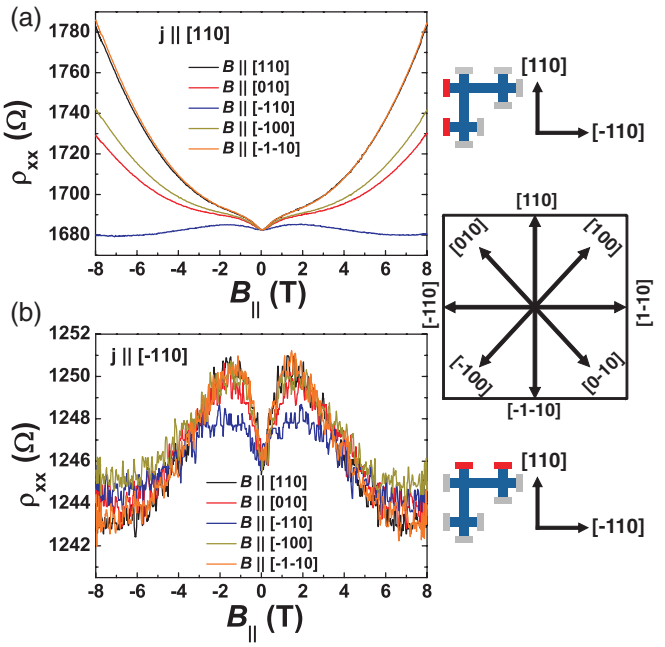

FIG. 8. (Color online) Longitudinal magnetoresistance at $T = 4.2$ K by rotating the magnetic field $B_\parallel$ within the sample plane. (a) Current $j \parallel [110]$: WAL signal and maximal PMR are observed for $B_\parallel$ along [110] and [$\bar{1}\bar{1}$0], whereas only WAL signal is present for $B_\parallel \parallel [\bar{1}10]$. The strength of PMR is intermediate for $B_\parallel$ along [010] and [$\bar{1}$00]. (b) Current $j \parallel [\bar{1}10]$: WAL signal observable for all orientations of $B_\parallel$. The sketches indicate the directions of B with respect to the Hall bar and crystal direction. The contacts used for the measurements are indicated in red.

the in-plane field unambiguously lowers the critical magnetic field denoting the transition from WAL to WL and increases the spin relaxation time from $\tau_{so} = 2.15$ ps at 0° to $\tau_{so} = 2.75$ ps at 88°. The phase coherence time τ_ϕ simultaneously increases from $\tau_\phi = 6.8$ ps to $\tau_\phi = 8$ ps. The increase in τ_{so} with increasing $B_\parallel$ indicates that the spin randomization is reduced and supports our former interpretation that the DP spin relaxation mechanism dominates. Similar behavior has been reported for 2DESs in InGaAs/InAlAs QW structures.[45] In systems with EY as the dominating mechanism, the opposite behavior, a reduction of τ_{so} on increasing $B_\parallel$, is expected.[43] The increase in τ_ϕ can be explained by squeezing of the wave function of the 2D holes by larger in-plane fields,[46] or it could be a sign that for large tilt angles the Zeeman energy and SOI energy are comparable.[45]

Along the [110] crystallographic direction, the transition from positive to negative magnetoresistance around $2H_{so}$ seems to have superimposed on it an even stronger positive magnetoresistance (PMR) for tilt angles $\alpha > 80°$. As displayed in the upper set of traces in Fig. 7, the PMR is strongly increased for tilt angles larger than 80°. A shoulder in ρ_{xx} is observed, roughly marking the value of $2H_{so}$, which seems to shift to lower $B_\perp$ values with increasing tilt angle, consistent with the finding for the [$\bar{1}$10] direction. We associate this PMR with transport through magnetic barriers resulting from the nonplanarity of the QW hosting the 2DHS.[47,48] The cross-hatched morphology caused by the metamorphic growth is more pronounced along the [110] direction, as observed in AFM images of the surface topology [Fig. 1(b)]. The relation between surface morphology and the undulating shape of the QW can further be seen from the lower hole mobility for currents along the [110] direction.

To shed light on the pronounced PMR and the influence of the anisotropic corrugation in the plane of the 2DHS, we have investigated the longitudinal magnetoresistance in the presence of an in-plane magnetic field $B_\parallel$. Therefore, additional magnetotransport measurements were carried out for magnetic field $B_\parallel$ rotated within the plane of the 2DHS. We have to distinguish between two principal configurations, with the magnetic field aligned parallel ($j \parallel B_\parallel$) or perpendicular ($j \perp B_\parallel$) to the current direction. Since the cross-hatched undulation and (related to this) the hole mobility are anisotropic between the [$\bar{1}$10] and the [110] crystallographic directions, the magnetoresistance for both directions was measured. The results are plotted for representative magnetic field configurations ($B_\parallel \parallel \langle 100\rangle$ and $\langle 110\rangle$) in Fig. 8 for (a) $j \parallel [110]$ and (b) $j \parallel [\bar{1}10]$. The contact configurations with respect to crystallographic directions are sketched adjacent to the panels.

For $j \parallel [110]$ [Fig. 8(a)], the WAL signal has a well pronounced PMR superimposed on it, if the external magnetic field is applied along [110] and [$\bar{1}\bar{1}$0], hence $j \parallel B_\parallel$. In contrast, for $j \parallel [110]$ and $j \perp B_\parallel$ only the WAL signature is observed. If $B_\parallel$ is neither parallel nor perpendicular to $j \parallel [110]$, the magnetoresistance is a superposition of the WAL signature and PMR, whereas the PMR is less pronounced than when $j \perp B_\parallel$. In the second arrangement, for $j \parallel [\bar{1}10]$ [see Fig. 8(b)], no significant PMR signal is revealed for any investigated direction of $B_\parallel$. The WAL signature is marginally reduced for $B_\parallel \parallel [\bar{1}10]$. We ascribe the superimposed PMR to classical motion of charge carriers through magnetic barriers formed by the undulated QW plane.[47–49]

Even if the external magnetic field is perfectly aligned parallel to the sample surface, the two-dimensional holes experience a nonzero perpendicular component of the magnetic field $B_\perp^{\text{eff}}$, because of the nonplanarity of the quantum well. The effective field $B_\perp^{\text{eff}}$ is spatially modulated following the undulating

shape of the 2DHS related to the cross-hatched morphology. Charge carriers traveling along the current path experience the inhomogeneous $B_{\perp}^{\text{eff}}$ and thus feel magnetic barriers.[49] They can pass those directly, if the initial velocity of the charge carriers perpendicular to the magnetic barriers is high enough. Charge carriers with lower velocity perpendicular to the barriers cannot propagate through them. They drift parallel to the barrier, a behavior caused by the value of $\boldsymbol{E} \times \boldsymbol{B}$. This explanation is consistent with the experimental data for $j \parallel [110]$. A PMR is observable for $B_{\parallel} \parallel j$ but not for $B_{\parallel} \perp j$ [Fig. 8(a)].

To explain phenomenologically why for $j \parallel [\bar{1}10]$ the PMR is absent for all angles between the current path and the in-plane aligned magnetic field, we consider two distinct and related properties of our heterostructure. The mobility and consequently the drift velocity are larger for holes traveling along the $[\bar{1}10]$ direction compared to the [110] direction and the modulation strength of $B_{\perp}^{\text{eff}}$ is reduced. This is because of different undulations along these two orthogonal crystal directions. The nonplanarity of the quantum film is directly connected to the surface morphology.[28] A measure of the surface roughness is the one-dimensional root mean square (rms) roughness, which can be determined from line scans of atomic force microscopy measurements of the surface. The averaged rms values are about 0.7 nm for the $[\bar{1}10]$ direction and about 2.9 nm for [110], with a maximal deviation of a single scan of $\pm 30\%$ [see also Fig. 1(b)]. The higher drift velocity together with the lower modulation strength of $B_{\perp}^{\text{eff}}$ are most likely sufficient that most of the holes propagating along the $[\bar{1}10]$ direction can pass the "smaller" magnetic barrier. The behavior is very similar for 2DESs confined in InAs-based heterostructures.[48] There a PMR is observed for both current directions and it seems to be much stronger than in our experiment. For a nonplanar 2DEG, the PMR is also stronger for the less mobile [110] direction and reduced for the higher-mobility $[\bar{1}10]$ direction.[48]

VI. CONCLUSION

In conclusion, we have investigated magnetotransport properties of Mn-modulation-doped, high-mobility 2DHSs. In addition to the typical two-dimensional behavior, including SdH oscillations and the quantum Hall effect, a WAL signature at low magnetic fields has been observed. The presence of the WAL demonstrates strong SOI in such heterostructures. Phase coherent transport is not destroyed for $T > 600$ mK by the presence of magnetic impurities separated by only a few nanometers from the itinerant holes. We have observed WAL signals for temperatures between 200 mK and 16 K and also in the presence of a parallel applied magnetic field. Below $T < 4.2$ K, the transverse resistance is a superposition of the normal Hall effect, AHE, and PHE and the longitudinal resistance a superposition of the WAL or WL signal and AMR indicating spontaneous magnetization in the material.

From HLN fits to the conductivity correction, characteristic phase τ_{ϕ} and spin relaxation times τ_{so} have been extracted and their temperature dependency as well as the influence of an applied in-plane magnetic field are discussed. From the temperature dependence of τ_{ϕ} and τ_{so} we infer that phase relaxation is caused by inelastic hole-hole interaction and the dominating spin relaxation mechanism is the Dyakonov-Perel mechanism. This assumption is strengthened by the observation that τ_{so} increases with increasing tilt angle in tilted magnetic fields. The values for τ_{ϕ} and τ_{so} are consistent with those given in the literature. For $T > 600$ mK, τ_{ϕ}^{-1} is directly proportional to the temperature and hence follows the theoretically expected trend for inelastic hole-hole interactions. At millikelvin temperatures, we found a deviation from the linear temperature dependence of τ_{ϕ}^{-1} that might be explained by the influence of the AMR present in ρ_{xx} or by an interaction with the Mn-doped DMS layer. The saturation of τ_{ϕ} could be further investigated by studying samples with different magnetic impurity concentrations in the Mn doping layer, gaining variations in the ferromagnetic transition temperature T_c.

The magnetoresistance at large in-plane magnetic fields (B almost parallel to the QW) reveals a superposition of the WAL signal and a positive magnetoresistance. This PMR is interpreted as a classical transport effect. The metamorphic growth causes a cross-hatched morphology leading to a nonplanar 2DHS. A magnetic field applied parallel to the QW simultaneously imprints a modulated perpendicular field that forms magnetic barriers that deflect carriers propagating parallel to $B_{\parallel}$ without sufficient velocity.

In further experiments, it might be interesting to tune the Rashba SOI term by changing the symmetry of the confinement potential, either *in situ* by applying an electric field perpendicular to the QW via the field effect or by growing QW structures with different symmetries of the confinement potentials hosting the 2DHS. The spin relaxation time is a key property for spintronic devices: an improvement of the spin relaxation time τ_{so} in the present magnetic 2DHS could be achieved by drastically lowering the width of the current channel down to a quasi-one-dimensional path as theoretically predicted[50] and experimentally reported for 2DESs.[51]

ACKNOWLEDGMENTS

We thank S. Kettemann, P. Wenk, and R. Dinter for stimulating discussions. This work was supported by the DFG via SFB 508 "Quantum Materials" and by the excellence initiative LEXI. U.W. and W.W. acknowledge the support by the DFG via SFB 689 "Spin Phenomena in Reduced Dimensions."

*Stefan.Knott@physnet.uni-hamburg.de

†Present address: Department of Physics, Columbia University, 538 West 120th Street, MC 5289, New York, NY 10027, USA.

[1] I. Zutic, J. Fabian, and S. Das Sarma, Rev. Mod. Phys. **76**, 323 (2004).

[2] S. A. Wolf, D. D. Awschalom, R. A. Buhrman, J. M. Daughton, S. von Molnár, M. L. Roukes, A. Y. Chtchelkanova, and D. M. Treger, Science **294**, 1488 (2001).

[3] D. D. Awschalom and M. Flatté, Nat. Phys. **3**, 153 (2007).

[4] H. Ohno, Science **281**, 951 (1998).

[5]Y. Ohno, D. Young, B. Beschoten, F. Matsukura, H. Ohno, and D. D. Awschalom, Nature (London) **402**, 790 (1999).
[6]X. Lou, C. Adelmann, S. A. Crooker, E. S. Garlid, J. Zhang, K. M. Reddy, S. D. Flexner, C. J. Palmstrom, and P. A. Crowell, Nat. Phys. **3**, 197 (2007).
[7]G. Dresselhaus, Phys. Rev. **100**, 580 (1955).
[8]E. I. Rashba, Sov. Phys. Solid State **2**, 1109 (1960).
[9]Y. A. Bychkov and E. Rashba, J. Phys. C **17**, 6039 (1984).
[10]R. Winkler, *Spin-Orbit Coupling Effects in Two-Dimensional Electron and Hole Systems* (Springer-Verlag, Berlin, 2003).
[11]B. Das, S. Datta, and R. Reifenberger, Phys. Rev. B **41**, 8278 (1990).
[12]E. A. de Andrada e Silva, G. C. La Rocca, and F. Bassani, Phys. Rev. B **50**, 8523 (1994).
[13]T. Schapers, G. Engels, G. Lange, T. Klocke, M. Hollfelder, and H. Luth, J. Appl. Phys. **83**, 4324 (1998).
[14]D. Grundler, Phys. Rev. Lett. **84**, 6074 (2000).
[15]S. Hikami, A. Larkin, and Y. Nagaoka, Prog. Theor. Phys. **63**, 707 (1980).
[16]G. Bergmann, Solid State Commun. **42**, 815 (1982).
[17]P. D. Dresselhaus, C. M. A. Papavassiliou, R. G. Wheeler, and R. N. Sacks, Phys. Rev. Lett. **68**, 106 (1992).
[18]T. Koga, J. Nitta, T. Akazaki, and H. Takayanagi, Phys. Rev. Lett. **89**, 046801 (2002).
[19]B. Grbić, R. Leturcq, T. Ihn, K. Ensslin, D. Reuter, and A. D. Wieck, Phys. Rev. B **77**, 125312 (2008).
[20]G. M. Minkov, A. A. Sherstobitov, A. V. Germanenko, O. E. Rut, V. A. Larionova, and B. N. Zvonkov, Phys. Rev. B **71**, 165312 (2005).
[21]D. Neumaier, K. Wagner, S. Geißler, U. Wurstbauer, J. Sadowski, W. Wegscheider, and D. Weiss, Phys. Rev. Lett. **99**, 116803 (2007).
[22]M. Ciorga, A. Einwanger, U. Wurstbauer, D. Schuh, W. Wegscheider, and D. Weiss, Phys. Rev. B **79**, 165321 (2009).
[23]U. Wurstbauer, M. Soda, R. Jakiela, D. Schuh, D. Weiss, J. Zweck, and W. Wegscheider, J. Cryst. Growth **311**, 2160 (2009).
[24]K. Morita, H. Sanada, K. Matsuzaka, C. Y. Hu, Y. Ohno, and H. Ohno, Physica E **21**, 1007 (2004).
[25]W. Desrat, F. Giazotto, V. Pellegrini, M. Governale, F. Beltram, F. Capotondi, G. Biasiol, and L. Sorba, Phys. Rev. B **71**, 153314 (2005).
[26]U. Wurstbauer and W. Wegscheider, Phys. Rev. B **79**, 155444 (2009).
[27]S. Löhr, S. Mendach, T. Vonau, C. Heyn, and W. Hansen, Phys. Rev. B **67**, 045309 (2003).
[28]D. Ercolani, G. Biasiol, E. Cancellieri, M. Rosini, C. Jacoboni, F. Carillo, S. Heun, L. Sorba, and F. Nolting, Phys. Rev. B **77**, 235307 (2008).
[29]H. X. Tang, R. K. Kawakami, D. D. Awschalom, and M. L. Roukes, Phys. Rev. Lett. **90**, 107201 (2003).
[30]T. Jungwirth, J. Sinova, J. Mašek, J. Kučera, and A. H. MacDonald, Rev. Mod. Phys. **78**, 809 (2006).
[31]T. S. Nunner, N. A. Sinitsyn, M. F. Borunda, V. K. Dugaev, A. A. Kovalev, A. Abanov, C. Timm, T. Jungwirth, J.-I. Inoue, A. H. MacDonald, and J. Sinova, Phys. Rev. B **76**, 235312 (2007).
[32]S. V. Iordanskii, Yu. B. Lyanda-Geller, and G. E. Pikus, JETP Lett. **60**, 206 (1994).
[33]K. K. Choi, D. C. Tsui, and S. C. Palmateer, Phys. Rev. B **33**, 8216 (1986).
[34]W. Knap, C. Skierbiszewski, A. Zduniak, E. Litwin-Staszewska, D. Bertho, F. Kobbi, J. L. Robert, G. E. Pikus, F. G. Pikus, S. V. Iordanskii, V. Mosser, K. Zekentes, and Y. B. Lyanda-Geller, Phys. Rev. B **53**, 3912 (1996).
[35]B. Altshuler, A. Aronov, and D. Khmelnitsky, J. Phys. C **15**, 7367 (1984).
[36]I. Garate, J. Sinova, T. Jungwirth, and A. H. MacDonald, Phys. Rev. B **79**, 155207 (2009).
[37]G. M. Alzoubi and N. O. Birge, Phys. Rev. Lett. **97**, 226803 (2006).
[38]Y. Niimi, Y. Baines, T. Capron, D. Mailly, F.-Y. Lo, A. D. Wieck, T. Meunier, L. Saminadayar, and C. Bäuerle, Phys. Rev. B **81**, 245306 (2010).
[39]B. L. Altshuler and A. G. Aronov, *Electron-Electron Interaction in Disordered Conductors* (Elsevier Science Publisher, Amsterdam, 1985), pp. 1–153.
[40]S. Chakravarty and A. Schmid, Phys. Rep. **140**, 193 (1986).
[41]T. Ihn, *Semiconductor Nanostructures: Quantum States and Electronic Transport* (Oxford University Press, Oxford, 2010).
[42]G. M. Minkov, A. V. Germanenko, O. E. Rut, A. A. Sherstobitov, L. E. Golub, B. N. Zvonkov, and M. Willander, Phys. Rev. B **70**, 155323 (2004).
[43]J. M. Kikkawa and D. D. Awschalom, Phys. Rev. Lett. **80**, 4313 (1998).
[44]F. E. Meijer, A. F. Morpurgo, T. M. Klapwijk, T. Koga, and J. Nitta, Phys. Rev. B **70**, 201307 (2004).
[45]F. E. Meijer, A. F. Morpurgo, T. M. Klapwijk, and J. Nitta, Phys. Rev. Lett. **94**, 186805 (2005).
[46]T. Chakraborty and P. Pietiläinen, Phys. Rev. B **39**, 7971 (1989).
[47]M. L. Leadbeater, C. L. Foden, J. H. Burroughes, M. Pepper, T. M. Burke, L. L. Wang, M. P. Grimshaw, and D. A. Ritchie, Phys. Rev. B **52**, R8629 (1995).
[48]S. Löhr, C. Heyn, and W. Hansen, Appl. Phys. Lett. **84**, 550 (2004).
[49]I. S. Ibrahim, V. A. Schweigert, and F. M. Peeters, Phys. Rev. B **56**, 7508 (1997).
[50]S. Kettemann, Phys. Rev. Lett. **98**, 176808 (2007).
[51]Y. Kunihashi, M. Kohda, and J. Nitta, Phys. Rev. Lett. **102**, 226601 (2009).